

## Volume-expansion-induced lattice instability and solid-state amorphization

K. Kusunoki

*Materials Physics Division, National Research Institute for Metals, 1-2-1 Sengen, Tsukuba-shi, Ibaraki 305, Japan*

(Received 26 July 1995)

Structural changes of elemental and binary thin-film layered crystals are investigated under coercive volume expansion using molecular-dynamics simulations. The results show that, although the crystalline lattice itself is stable against large volume expansion, it can be easily changed into a disordered structure when small anisotropic forces are locally applied. This type of lattice instability may be responsible for triggering the so-called solid-state amorphization.

Recently, there has been an enormous number of reports<sup>1</sup> on so-called solid-state amorphization (SSA), i.e., spontaneous amorphization of crystalline systems. Most of them refer to experimental works, such as irradiation, diffusion of thin-film layers, rolling, and mechanical processing of both elemental and alloy powders. General characteristics of this somewhat curious phenomenon are, as have been repeatedly mentioned, (i) a large negative heat of mixing between constituent elements, (ii) a large diffusivity of atoms of one element into the other elemental crystal, and (iii) a large atom size difference between the constituents. With these basic features, several authors have made theoretical considerations on the occurrence of SSA. Schultz<sup>2</sup> states, for the case of annealing diffusion couples, that a local destabilization of the crystalline phase caused by an interdiffusion reaction gives rise to an amorphous phase formation. Desre<sup>3</sup> and Zheng<sup>4</sup> insist, from a thermodynamic aspect, that the driving force from an initially sharp concentration gradient contributes to solid-state amorphization rather than formation of an intermetallic at the interface of the crystal. In the case of mechanical processing, it is insisted<sup>5</sup> that the SSA reaction could possibly result from the presence of point or line defects introduced during plastic deformation. In every case, the occurrence of the SSA reaction in the systems showing the above basic features is considered to be caused by a large negative heat of mixing between constituent elements.<sup>6</sup> There is one exception, multilayers of Al and Pt, which does not meet these characteristics, but spontaneously amorphizes.<sup>7</sup> There have been also reports of another type of SSA, in which a crystalline solid solution such as Cr-Ti can spontaneously amorphize upon low-temperature annealing. The occurrence of this type of SSA is usually discussed in terms of lattice softening.<sup>8</sup> These findings indicate that considerations not only of the heat of mixing but also of the lattice instability are important for a general interpretation of SSA. In this regard, previous results of molecular-dynamics simulations on defect-induced SSA of uniform materials<sup>9-12</sup> have been interpreted in terms of a lattice destabilization, again revealing the importance of the lattice instability.

In connection with the above, the volume expansion of a crystal, in other words, cooperative displacements of the atoms from their equilibrium positions, will cause a lattice instability by increasing the potential energy of the crystal. The present study is intended to examine whether a crystal can change into an amorphous phase by volume expansion,

and for this purpose, we performed molecular-dynamics simulations in two ways. One of them is a volume expansion of a single crystal under uniaxial stress. The other is a volume expansion of multilayered thin-film crystals consisting of different elements. In the latter case, we can expect that the differently sized particles at the interfaces of the multilayer play some role in the destabilization of the lattice structure during the volume expansion. For simplicity, we use a modified Lennard-Jones-type interatomic potential

$$\phi(r_{ij}) = \varepsilon \left[ \left( \frac{\sigma}{r_{ij}} \right)^8 - \left( \frac{\sigma}{r_{ij}} \right)^4 \right] + \alpha r_{ij} + \beta, \quad (1)$$

where  $r_{ij}$  is the distance between particles  $i$  and  $j$ , and  $\alpha$  and  $\beta$  are parameters introduced so that the potential and its derivative vanish at a truncation distance  $R_c$ , equal to the fourth nearest-neighbor distance of a fcc lattice.

In the case of the volume expansion of a single crystal, we use potential parameters which reproduce well the lattice parameter and the cohesive energy of fcc lanthanum. This interatomic potential, denoted A-A, is shown in Fig. 1. The single crystal, consisting of 2842 particles (sized  $7 \times 7 \times 14$  in units of the lattice parameter  $a = 5.302 \text{ \AA}$ ), is extended at a reduced temperature of  $T^* = 0.0129$  ( $T^* = k_B T / \varepsilon_{AA}$ , where  $T$  is 600 K and  $k_B$  is Boltzmann's constant) with a speed of  $0.0025a/\tau$  ( $\tau = 0.196 \text{ ps}$ ) along the  $Z$  direction, keeping the

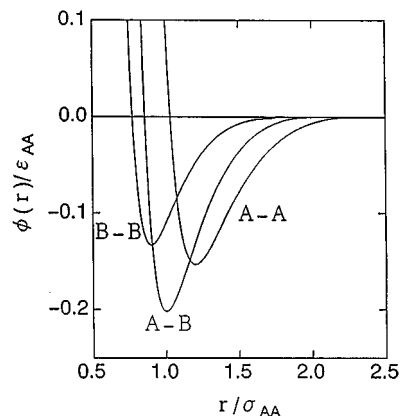


FIG. 1. Interatomic potentials calculated from the cohesive energies and the lattice parameters of fcc La (A), fcc Au (B), and their intermetallic compounds.

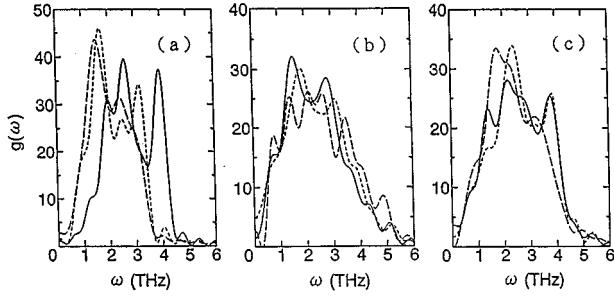


FIG. 2. Phonon frequency distributions calculated from the velocity autocorrelation function. (a) Solid, dotted, and dashed lines are for 0%, 14.4%, and 17.4% volume expansion of the single crystal consisting of particles A, respectively. (b) and (c) show those for the particles A and B in the multilayer system at times  $6.0 \times 10^7 \tau$  ( $\tau = 0.196$  ps) (solid lines),  $1.2 \times 10^7 \tau$  (dotted lines), and  $1.8 \times 10^7 \tau$  (dashed lines).

cross-sectional area constant, applying spatial periodical boundary conditions to the  $X$  and  $Y$  directions. In this case every particle in the uppermost and lowermost planes, which are perpendicular to the  $Z$  direction, is oppositely stretched along the  $Z$  direction. The results show that the crystal reacts elastically up to about a 15% volume expansion, after which it deforms plastically. Phonon frequency distributions calculated from velocity autocorrelation functions of the particles for 0%, 14.4%, and 17.4% volume expansions are shown in Fig. 2(a), where it is seen that the contributions at lower frequencies become more pronounced as the volume increases. This indicates the occurrence of lattice softening. However, it is shown in this case that the lattice softening cannot cause the structure to disorder, but only cause plastic deformation.

In the case of the volume expansion of a multilayered crystal, we use two types of elemental crystals, A and B. Crystal A consists of the same particles used in the volume expansion of the single crystal, and crystal B consists of particles with an interatomic potential  $B-B$  fit to reproduce both the lattice parameter and the cohesive energy of a fcc crystal of gold. Parameters for the cross interaction  $A-B$  are calculated so that both the lattice parameters and cohesive energies estimated from Miedema's rule,<sup>13</sup> of the lanthanum-gold intermetallic compounds  $AB$  ( $Bf$  type) and  $A_2B$  ( $C37$  type), are reproduced. In the course of the above calculations, we made slight modifications to the potential parameters so that the lattice-parameter ratio of A to B is 4:3, which value is convenient for constructing a system with spatial periodical boundary conditions. These modifications were done to eliminate misfits in constructing the multilayered crystal. The potential parameters are listed in Table I, and the potentials are shown in Fig. 1. The distance which gives a

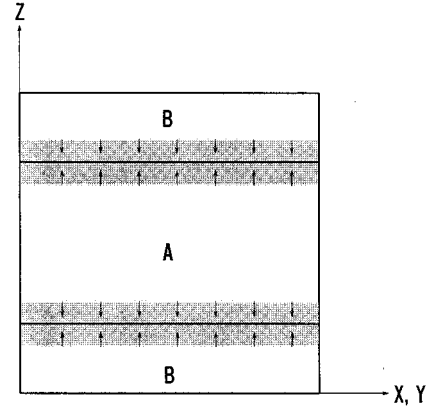


FIG. 3. Schematic view of the simulation box with constant edge length throughout the simulation. After, when alloying takes place between A and B according to  $\Delta H_{\text{mix}} < 0$ , the netted zones shrink according to  $\Delta V_{\text{mix}} < 0$ , and consequently, volume expansion occurs in the rest of the crystals in the simulation box.

minimum value to the  $A-B$  potential is shorter by 4.5% than the average of the distances which give minimum values to the  $A-A$  and  $B-B$  potentials. It should be noted that the average atomic volume of the intermetallic compounds of the lanthanum-gold system is smaller by about 3% than that of the constituent atoms.<sup>14</sup> This negative excess volume of mixing ( $\Delta V_{\text{mix}}$ ) is also the case for the present system. The average atomic volume of a CsCl-type equiatomic compound, relaxed with the above potentials, is calculated to be smaller by 11.4% than the average atomic volume of crystals A and B, and the excess enthalpy of mixing ( $\Delta H_{\text{mix}}$ ) between A and B is calculated to be  $-1.81 \times 10^{-12}$  erg per atom. A multilayer system is constructed with an A-type crystal sandwiched between two B-type crystals.

Under the above conditions for the potentials, alloying between the crystals will occur at the interface, and consequently, volume shrinkage will be provoked around the interface at which an alloying reaction takes place. So, if the size of the simulation box is kept unchanged throughout the simulation, it is possible that the major part of the crystals in the multilayer system, excluding the minor part of the crystals very close to the interface, is expanded. This is schematically shown in Fig. 3. In the present system, crystal A contains 576 particles and, each of the crystal B, 480 particles with a periodical boundary condition for all directions. Both the (100) plane and [100] direction of crystals A and B are set parallel. A (013) plane of crystal A and a (031) plane of crystal B are set to contact each other as well [see Fig. 4(a)]. At the beginning of the simulation, the present system has 12 (100) planes perpendicular to the  $X$  axis for crystal A and 16 for each of the crystals B. Prior to the simulation run, the

TABLE I. Potential parameters for the present system.

Type	$\varepsilon$ ( $10^{-12}$ erg)	$\sigma$ ( $\text{\AA}$ )	$\alpha$ ( $10^{-13}$ erg/ $\text{\AA}$ )	$\beta$ ( $10^{-12}$ erg)	$R_c$ ( $\text{\AA}$ )
A-A	6.405955	3.272249	-1.118265	1.062351	7.5425
B-B	5.482744	2.454187	-1.276138	0.909247	5.6569
A-B	7.838028	2.738161	-1.324227	1.099313	6.5997

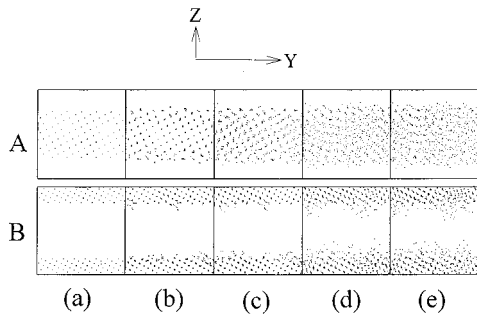


FIG. 4. Time evolution of the snapshots of the particle positions in the multilayer system, projected onto the  $Y$ - $Z$  plane. (a)  $0\tau$ , (b)  $1.0 \times 10\tau$ , (c)  $3.0 \times 10\tau$ , (d)  $6.0 \times 10^2\tau$ , and (e)  $1.8 \times 10^3\tau$ .

spacings between the crystals are set so that the total potential energy of the system is a minimum at 0 K.

The results are as follows. As soon as the simulation began, crystals  $A$  and  $B$  reacted at the interface of the multilayer system, emitting heat which is produced by the large negative excess enthalpy of mixing between  $A$  and  $B$ . In the course of the reaction, both  $A$  and  $B$  are, as was expected, seen to expand along the  $Z$  axis. This is shown in Fig. 4, which depicts the snapshots of the particles positions  $A$  and  $B$  separately. The volume expansion of  $A$  is more pronounced than that of  $B$ . The reason why the  $A$  crystals have preferentially undergone a volume expansion is easily understood by comparing the curvatures of the potentials at their equilibrium positions (see Fig. 1). That is, the curvature of the  $A$ - $A$  potential is more dull compared to that of the  $B$ - $B$  potential.

Within a very short time of about  $6 \times 10^2\tau$  from the beginning of the simulation, crystal  $A$  has turned amorphous [see Fig. 4(d)]. The very rapid and initial relaxation [at  $10\tau$ , Fig. 4(b)] of crystal  $A$  is caused by the combined action of both the lattice expansion and an asymmetrical deformation in the vicinity of the interface between crystals  $A$  and  $B$ . This local deformation is promoted by the presence of differently sized particles at the crystal interfaces and is considered to give anisotropic forces on crystal  $A$ . Contrary to the case of crystal  $A$ , crystal  $B$  is composed of particles which are more strongly bound than particles  $A$ . Consequently, it is considered that the amorphization of crystal  $B$  does not occur simultaneously with that of crystal  $A$ . The movements of the particles during the very early stage of the initial reaction are shown in Fig. 5, where the trajectories of the particles, which are initially on a same plane perpendicular to the  $X$  axis, are shown for a time interval between 0 and  $6 \times 10^2\tau$ . (In these figures, the initial particle positions are at the centers of the large circles for  $A$  and of the small circles for  $B$ .)

It should be mentioned again that not crystal  $B$ , but only crystal  $A$  is amorphized during the very early stage of the relaxation not only at around the  $A/B$  interface, but also inside the whole area where particles  $B$  do not exist. So the amorphization process in the present system is obviously quite different from the one insisted by Desré<sup>3</sup> and Zheng.<sup>4</sup> The present results are—although the large negative heat of mixing plays an important role on attracting the different atoms at the interfaces of multilayered crystalline materials—indicative of the crystal-to-amorphous phase

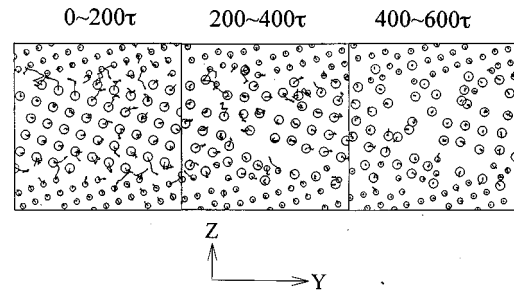


FIG. 5. Trajectories of the particles in the multilayer system for the time interval  $(0-600)\tau$ . The particles initially located on a plane perpendicular to the  $X$  axis are projected onto the  $Y$ - $Z$  plane. The initial particle positions are at the centers of the large circles for  $A$  and of the small circles for  $B$ .

transformation being triggered essentially by only a small cooperative but asymmetrical displacement of atoms from their equilibrium positions.

In Figs. 2(b) and 2(c), the time evolution of the phonon frequency distributions deduced of particles  $A$  and  $B$  are shown for times  $6.0 \times 10\tau$ ,  $1.2 \times 10^2\tau$ , and  $1.8 \times 10^3\tau$ , respectively. In the case of particles  $A$  [see Fig. 2(b)], the difference between the peak heights at lower and higher frequencies is observed to increase as time passes from  $6.0 \times 10\tau$  to  $1.2 \times 10^2\tau$ . This reveals the occurrence of lattice softening and subsequent disordering of crystal  $A$ . The various phonon frequency modes, which are seen to appear at time  $1.8 \times 10^3\tau$ , after the initial large relaxation is completed, may be caused by a finite-size effect of the present system. An overall shift of the intermediate-frequency region towards

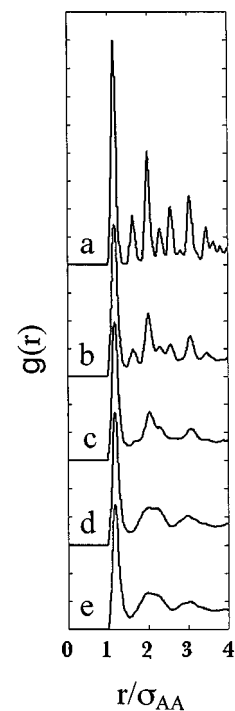


FIG. 6. Partial radial distribution functions of the  $A$ - $A$  pairs at times (a)  $0\tau$ , (b)  $1.0 \times 10\tau$ , (c)  $3.0 \times 10\tau$ , (d)  $6.0 \times 10^2\tau$ , and (e)  $1.8 \times 10^3\tau$ , corresponding to the snapshots in Fig. 4.

the higher-frequency region is caused mainly by an increase in the number of  $A$ - $B$  pairs, which are more tightly bound than the  $A$ - $A$  pairs. The time evolution of the phonon frequency distribution of particles  $B$  [see Fig. 2(c)] from  $6.0 \times 10^2 \tau$  to  $1.2 \times 10^2 \tau$  is rather similar to that for the case of the volume expansion of the single crystal [see Fig. 2(a)]. This similarity shows that the majority of particles  $B$  feels similar forces as the single crystal does during its initial volume expansion. However, interdiffusion between  $A$  and  $B$  causes, as can be seen from Fig. 4(e), moderate amorphization of crystal  $B$  after a long time. This is consistent with the fact that the peak at higher frequencies in the phonon frequency distribution of particles  $B$  is diminished as time passes from  $1.2 \times 10^2 \tau$  to  $1.8 \times 10^3 \tau$ . The partial radial distribution functions of particles  $A$  corresponding to the snapshots in Fig. 4 are shown in Fig. 6, in which the second-peak splitting characteristic of amorphous structures is observed to appear after the amorphization is complete [see Fig. 6(d)].

Generally speaking, not all the annealing of real diffusion couples can be done under the local volume-expansive (or the constant total-volume) condition. So the present results may not be directly applicable to the interpretation for the onset of SSA occurring in the multilayers of real lanthanum-gold samples.<sup>15</sup> However, there might be some situations where the present mechanism, a combination of cooperative lattice softening and the localized asymmetrical deformation, is indeed relevant. Possible situations are, for instance, rolling and mechanical alloying of multilayered crystalline materials. Under such a severe mechanical treatment accompanied by heavy deformations, not only compressive, but also large extensive forces must be applied to the materials. Such extensive forces will cause an adiabatic volume expansion in addition to the plastic deformation of the crystalline lattice. In connection with this, as examined in the present study, diffusion couples can possibly undergo SSA under special constraints or configurations.

<sup>1</sup>Proceedings of the Sixth International Conference on Rapidly Quenched Metals, Montreal, 1987 [Mater. Sci. Eng. **97** (1988)]; Proceedings of the Conference on Solid State Amorphizing Transformations, Los Alamos, 1987 [J. Less-Common Met. **140** (1988)]; Proceedings of the Seventh International Conference on Liquid and Amorphous Metals, Kyoto, 1989 [J. Non-Cryst. Solids **117/118** (1990)]; Proceedings of the International Conference on Amorphization by Solid State Reaction, 1990 [J. Phys. (Paris) Colloq. **51**, C4 (1990)]; Proceedings of the Eighth International Conference on Liquid and Amorphous Metals, Wien, Austria, 1992 [J. Non-Cryst. Solids **156–158** (1993)]; J. Alloys and Compounds, **194** (1993) (special issue on solid state amorphizing transformations).

<sup>2</sup>L. Schultz, Philos. Mag. B **61**, 453 (1990).

<sup>3</sup>P. J. Desré, Acta Metall. **39**, 2309 (1991).

<sup>4</sup>Y. Zheng, Phys. Rev. B **45**, 7451 (1992).

<sup>5</sup>R. B. Schwartz and C. C. Koch, Appl. Phys. Lett. **49**, 149 (1986).

<sup>6</sup>W. L. Johnson, Prog. Mater. Sci. **30**, 81 (1986).

<sup>7</sup>B. Blanpain, L. H. Allen, J.-M. Legresy, and J. W. Mayer, Phys. Rev. B **39**, 13 067 (1989).

<sup>8</sup>A. Blatter, J. Gfeller, and M. von Allmen, J. Less-Common Met. **140**, 317 (1988).

<sup>9</sup>Y. Limoge, A. Rahman, H. Hsieh, and S. Yip, J. Non-Cryst. Solids **99**, 75 (1988).

<sup>10</sup>H. Hsieh and S. Yip, Phys. Rev. B **39**, 7476 (1989).

<sup>11</sup>C. Massobrio, V. Pontikis, and G. Martin, Phys. Rev. B **41**, 10 486 (1990).

<sup>12</sup>J. S. Tse and D. D. Klug, Phys. Rev. B **70**, 174 (1993).

<sup>13</sup>A. R. Miedema, F. R. de Boer, and P. F. de Chatel, J. Phys. F **3**, 1558 (1973).

<sup>14</sup>O. D. McMasters, K. A. Gshneidner, Jr., G. Bruzzone, and A. Palenzona, J. Less-Common Met. **25**, 135 (1971).

<sup>15</sup>R. B. Schwartz and W. L. Johnson, Phys. Rev. Lett. **51**, 415 (1983).